Received: 26 April 2022 | Revised: 31 January 2023 | Accepted: 15 February 2023

DOI: 10.1002/ldr.4659

RESEARCH ARTICLE

WILEY

Spatiotemporal variability of the potential wind erosion risk in Southern Africa between 2005 and 2019

Florian Kestel[1] | Monika Wulf[1,2] | Roger Funk[1]

[1]Working Group: Soil Erosion and Feedback in Research Area 1 "Landscape Functioning", Leibniz Centre for Agricultural Landscape Research (ZALF), Müncheberg, Germany

[2]Institute of Biochemistry and Biology, University of Potsdam, Potsdam, Germany

Correspondence
Florian Kestel, Working Group: Soil Erosion and Feedback in Research Area 1 "Landscape Functioning", Leibniz Centre for Agricultural Landscape Research (ZALF), Eberswalder Str. 84, 15374 Müncheberg, Germany.
Email: florian.kestel@zalf.de

Funding information
Bundesministerium für Bildung und Forschung; German Federal Ministry of Education and Research (BMBF), Grant/Award Number: 01LL1803B

Abstract

Regional assessments of the wind erosion risk are rare and vary due to the methods used and the available data to be included. The adaptation of existing methods has the advantage that the results can be compared directly. We adopted an already successfully applied methodology (ILSWE—applied in East Africa), to investigate the spatiotemporal variability of the wind erosion risk between 2005 and 2019 in Southern Africa. The approach integrates climatic variables, a vegetation index, and soil properties to describe the potential impact of wind erosion at the landscape scale. The annual and seasonal variability is determined by the vegetation cover, whereas droughts and strong El Niño events had only regional effects. We estimated that 8.3% of the study area experiences a moderate to elevated wind erosion risk over the 15-year period with annual and inter-annual fluctuations showing a slight upward trend. In general, the desert and drylands in the west have the highest proportion of risk areas, the moist forests in the east are characterized by a very low risk of wind erosion, while the grasslands, shrublands, and croplands in the interior most likely react to changes of climatic conditions. The validation process is based on a comparison with the estimated frequency of dust storms derived from the aerosol optical depth and angstrom exponent and revealed an overall accuracy of 65%. The results of this study identify regions and yearly periods prone to wind erosion to prioritize for further analysis and conservation policies for mitigation and adaptation strategies.

KEYWORDS
environmental modelling, geographic information systems, ILSWE model, remote sensing, temporal variability, wind erosion

1 | INTRODUCTION

In the 21st century, soil erosion is globally one of the most serious natural hazards, which challenges the environment, agricultural productivity, and thus food security (Montanarella et al., 2016; Montgomery, 2007). In arid and semi-arid regions wind erosion accounts for 46% of total land degradation (Zheng, 2009). Wind erosion is also a threat to Southern Africa favored by dry climates and seasonal droughts, affecting natural and anthropogenic-influenced sensitive biomes (Huang et al., 2016; Zhao et al., 2021). Against a backdrop of increasing population in the area and regional food production already reaching its natural limits, wind erosion-induced declines in soil fertility will put further pressure on crop production and ecosystem services and drive up economic costs (Department of Environmental Affairs, 2014; Kirui & Mirzabaev, 2014; Kotze & Rose, 2015). Additional anthropogenic drivers such as deforestation,

overgrazing, monocultures, large fields, and generally poor soil management can accelerate the process of wind erosion (UNEP, 2015; Webb et al., 2020). The vulnerability of soils to erosion by wind is affected by certain primary soil characteristics like grain size distribution, lime and carbon content, affecting secondary soil characteristics such as aggregate stability, soil surface crusting and roughness, or moisture levels (Funk et al., 2008; Shao, 2008; Wiesmeier et al., 2012). Additional dynamic factors are vegetation cover (VC) and climatic variability (Shao, 2008).

Studies have shown that emitted dust contains the finest and most valuable parts of soil, such as the silt and clay fraction and soil organic carbon (Funk et al., 2008; Ravi et al., 2011; Sterk et al., 1996). Soil organic carbon content of eroded dust can spike up to 17-times from its original source (Nerger et al., 2017). With wind erosion occurring in regions with a low net primary production, the loss of soil organic carbon can be considered an irrecoverable loss to soil quality (Chappell et al., 2016; Yan et al., 2005). Global dust emissions are estimated at 2000 Mt, of which 1500 Mt are deposited on land and 500 Mt in the oceans (Shao et al., 2011). While positive off-site effects are ocean and land fertilization, the loss of nutrients and organic matter increases the vulnerability of the source areas. If erosion rates exceed the rate of soil formation, it can push ecosystems to a state of decay (D'Odorico et al., 2013; Obalum et al., 2012; Zabel et al., 2014). The future prospect of climate change puts further pressure on regions prone to wind erosion, leading to a decrease in VC and biomass production (Munson et al., 2011; Ravi et al., 2010).

In the 1930s, Dust Bowl events in the Great Plains region of the United States triggered the development of empirical wind erosion models (Tatarko et al., 2013). Continuous efforts led to the wind erosion equation (WEQ), the first empirical model, based on wind tunnel experiments and field measurements, integrating different factors, for assessing annual soil loss (Woodruff & Siddoway, 1965). The revised WEQ (RWEQ) replaced WEQ as a tool to estimate erosion (Fryrear et al., 2001) and has been extensively tested and found to be in good agreement with on-field measurements (Buschiazzo & Zobeck, 2008). One of the more recent wind erosion models is a pan-European assessment, utilizing the most influential parameters that affect the potential of wind erosion on landscapes (Borrelli et al., 2016). This approach, the index of land susceptibility to wind erosion (ILSWE), has been adopted and modified by Fenta et al. (2020) for the East African region, with a high resolution of 100 m cell size and a validated accuracy of around 70%.

Research related to soil degradation in Southern Africa has been mainly focused on water erosion at the plot or watershed scale (Le Roux et al., 2008, 2007; Weinzierl et al., 2016). While there are studies on dust emissions in the South African Free State, information on a regional scale is rather lacking (Eckardt et al., 2020; Wiggs & Holmes, 2011). In general, focusing on one area alone does not provide a comprehensive view of the process of wind erosion in the Southern African region. This situation calls for a qualitative approach to map out areas most susceptible to wind erosion to narrow the knowledge gap and generate a basis for further studies.

In this study, the aim is to outline the general land susceptibility to wind erosion in the region of Southern Africa with the approved modeling approach ILSWE by integration of high-resolution remote sensing data and spatial analysis tools in a geographic information system (GIS). The specific goals are as follows:

1. To identify and highlight risk areas.
2. To analyze the annual spatial patterns, over a period of 15 years, to estimate a prospective trend.
3. To relate results to major types of land cover and predominant terrestrial ecoregions in the global warming context.

The results can give an impact on future erosion control management policies and land use scenarios. It will also provide environmental researchers with a basis for small-scale studies on the effects of wind erosion in the Southern African region.

2 | STUDY AREA

The investigated area covers the southern part of the African continent and includes seven countries: Namibia, Botswana, Zimbabwe, Mozambique, Eswatini, South Africa, and Lesotho comprising 3.9 million km^2 (Figure 1). About 11% or 433,619 km^2 of the area is under agricultural use. Southern Africa, as a terrestrial ecoregion, is dominated by savannas occupying 45% of its area, followed by desert and xeric shrublands with 35% coverage, respectively. While the western dry regions are poor in vegetation, the Cape and southern coastal areas have rich flora, ranging from small shrubs to Mediterranean woodlands. Moist broadleaf forests and mangroves characterize the humid east (Figure 1) (Burgess et al., 2004). The western regions are dominated by sandy soils, while the eastern regions are characterized by loamy soils (Figure 2).

The mean annual precipitation ranges between 5 mm on the west coast up to 1950 mm in the eastern regions with high inter-annual variability (Fauchereau et al., 2003) (Figure 3). The mean annual temperature is around 17°C, ranging from more than 40°C in the desert regions of Namibia and Botswana to −20°C in the high-altitude regions around Lesotho and Zimbabwe (Hijmans et al., 2005).

Observed trends in annual average near-surface temperature in Southern Africa, based on CRUTEM4v data, show a significant positive anomaly in comparison to the long-term average of 1961–1990, with the 2000s being the warmest decade (Engelbrecht et al., 2015; Osborn & Jones, 2014). This trend is more prevalent in minimum temperature, resulting in a limited diurnal temperature range (New et al., 2006). The El Niño-Southern Oscillation also affects Southern Africa and is generally associated with lower-than-normal rainfall, while strong events coincide with high drought severity (Philippon et al., 2012).

The region-wide average wind speed is 3.5–6.5 m s^{-1} reaching its highest in the mountainous country of Lesotho and the southern coastal area of South Africa and its lowest at the coast of Mozambique (Figure 3). The general wind direction is east, while westerly winds dominate on the southern coast in the summer months (Rienecker et al., 2011).

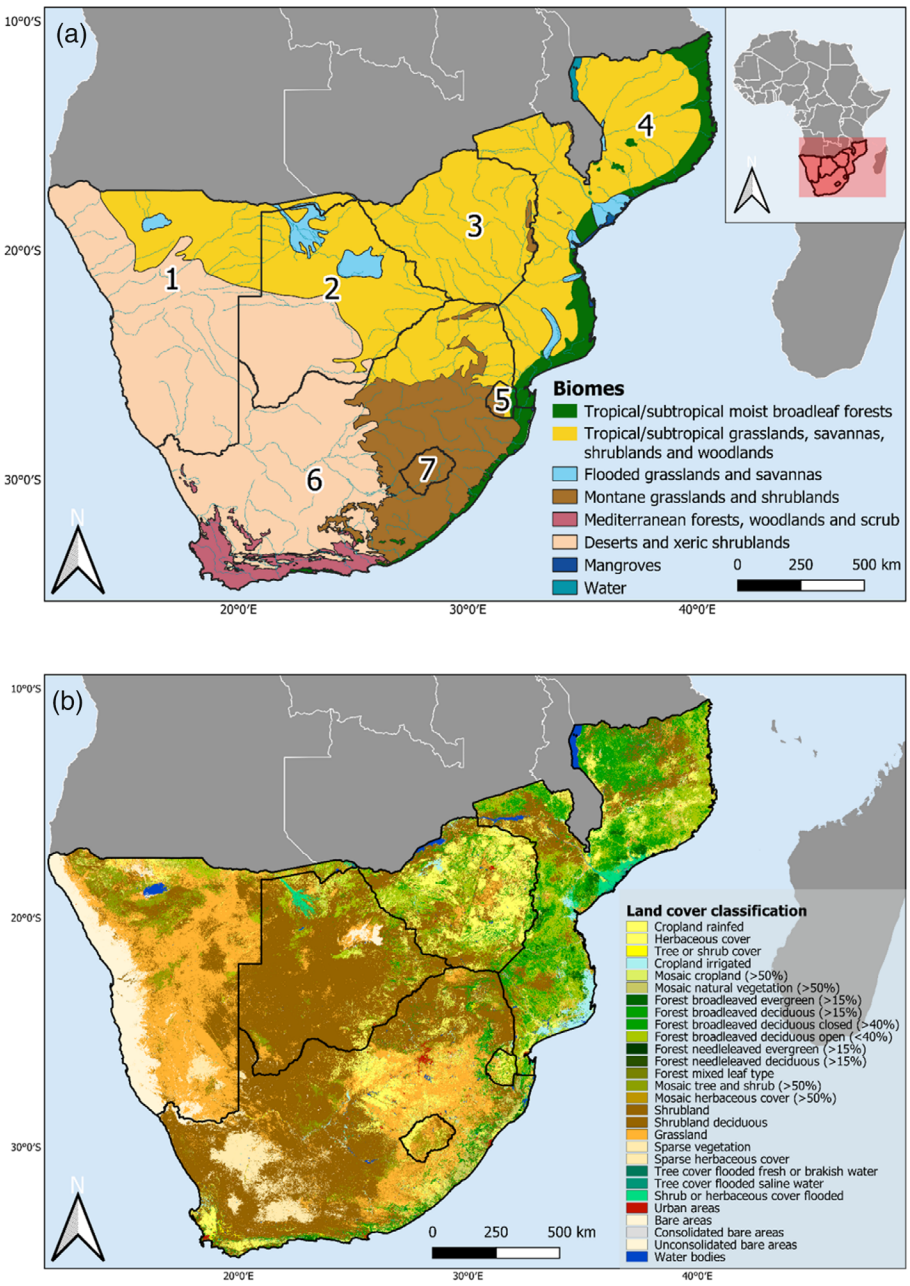

FIGURE 1 (a) Main biomes of Southern Africa comprising countries of the study area. Localized by numbers: (1) Namibia, (2) Botswana, (3) Zimbabwe, (4) Mozambique, (5) Eswatini, (6) South Africa, and (7) Lesotho (modified after Olson et al., 2001) and (b) land cover classification of the study area (ESA CCI). [Colour figure can be viewed at wileyonlinelibrary.com]

3 | MATERIALS AND METHODS

3.1 | Index of land susceptibility to wind erosion

The complexity of the wind erosion processes demands integration of a variety of physical parameters, which impede an adequate upscaling of plot-sized models (Funk & Reuter, 2006). Plot-sized models can have a demand for extensive data to meet requirements, which poses difficulties even on a local scale. It is necessary to reduce the parameters to the essentials, while adhering to well-established conditions for wind erosion, for a regional scale assessment (Böhner & Köthe, 2003). Therefore, macroscale-sized models are limited by the availability of spatially and temporally uniform datasets and call for modification and incorporation of varying data sources, measurement intervals, and periodicity. The approach in this study, the ILSWE (Borrelli et al., 2016) and its adaptation by Fenta et al. (2020) use static and dynamic erosion parameters. It inherits the basic three rules that wind erosion occurs when wind speed exceeds a threshold, the soil surface is susceptible and there is little to no vegetation (Tsoar, 1994). The factors used in the GIS analysis are divided into five categories to characterize the factorial and combined sensitivity to wind erosion: climatic erosivity (CE), wind-erodible fraction (EF), soil crust (SC), VC, and surface roughness (SR). To create a uniform relationship, the contributing factors were divided into a value range from 0 to 1 using the fuzzy logic approach. Fuzzy logic was introduced by Zadeh (1965) as a more realistic depiction of a range of metrics, in contrast to classic Boolean logic, distinguishing between false and true (McBratney & Odeh, 1997). The analysis was carried out, using ArcGIS (ArcMap 10.8.1, ESRI Inc., CA, USA), describing the established direct relationships between each individual erosivity factor to the rate of

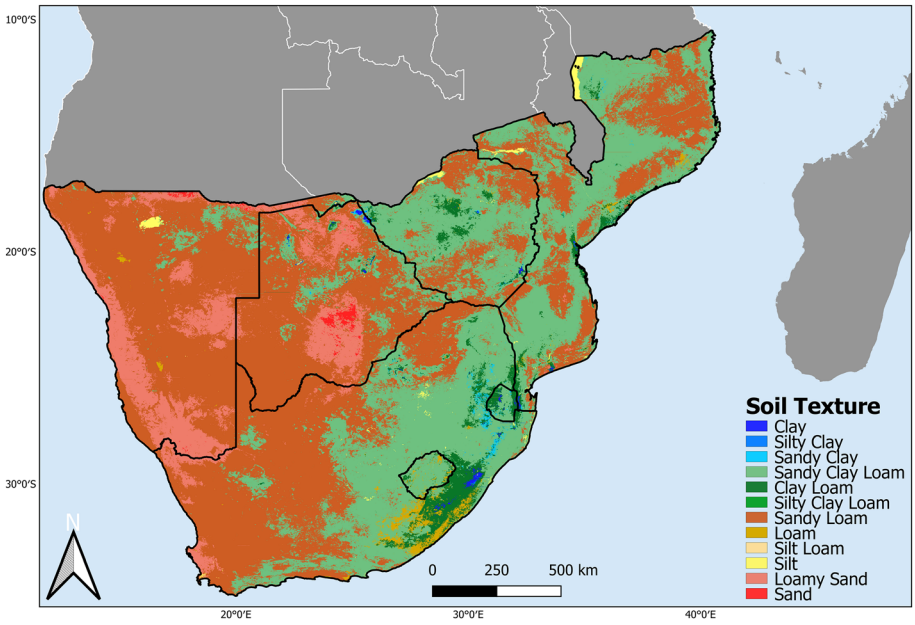

FIGURE 2 Soil texture classes of the study area after the United States Department of Agriculture (USDA) classification. [Colour figure can be viewed at wileyonlinelibrary.com]

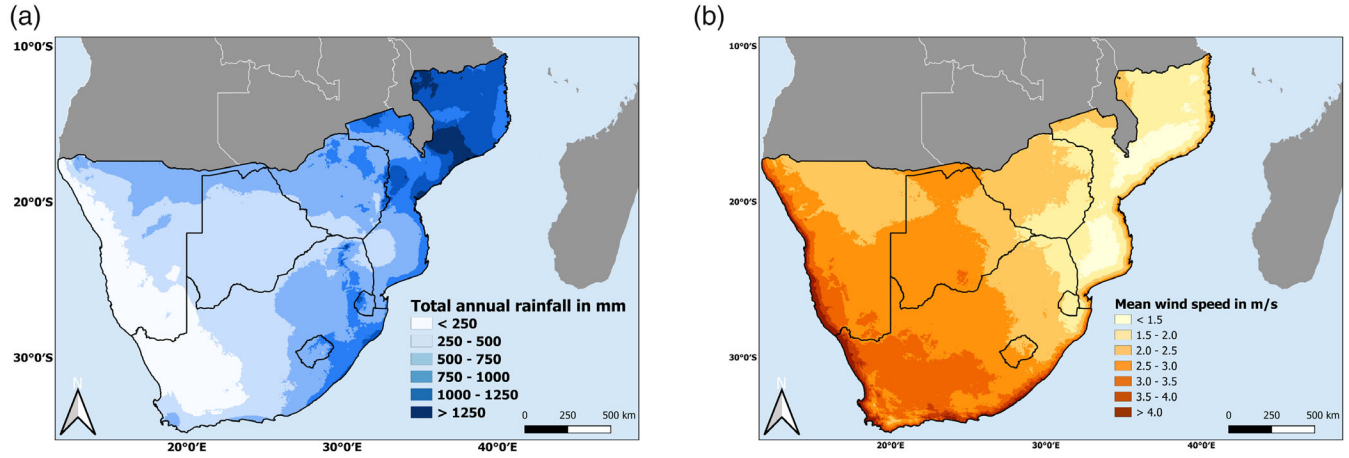

FIGURE 3 (a) Total annual rainfall and (b) mean wind speed over the study area between 2005 and 2019. [Colour figure can be viewed at wileyonlinelibrary.com]

wind erosion by fuzzy membership functions (Huete et al., 2002; Klik, 2004; USDA, 2002; Wever, 2012). The applied functions were as follows

1. Linear for CE, EF, and SC.
2. Exponential equivalent for VC.
3. Inverse logarithmic for SR.

Thus, a sensitivity assessment layer was produced for every factor separately to compute a summary map by multiplying each factor after Fenta et al. (2020):

$$\mathrm{ILSWE} = \mathrm{CE}^{*}\,\mathrm{EF}^{*}\,\mathrm{SC}^{*}\,\mathrm{VC}^{*}\,\mathrm{SR} \quad (1)$$

In the final step, the result was classified into five categories from very low to very high sensitivity by applying the Jenks–Caspall-algorithm. This classification method seeks to reduce the variance within classes and maximizes the variance between classes (Jenks & Caspall, 1971). The ILSWE was calculated for the 15-year period of 2005 to 2019, as well as each individual year. Furthermore, a seasonal index was created to highlight the most vulnerable periods throughout the year. Finally, an aerosol optical depth-based validation method was applied. The methodological structure is presented in Figure 4.

3.2 | Data sources

The datasets used for the GIS analysis and its validation are derived from the following sources (Table 1):

1. Wind speed, precipitation, and potential evapotranspiration are derived from TerraClimate, a monthly temporal climatic dataset

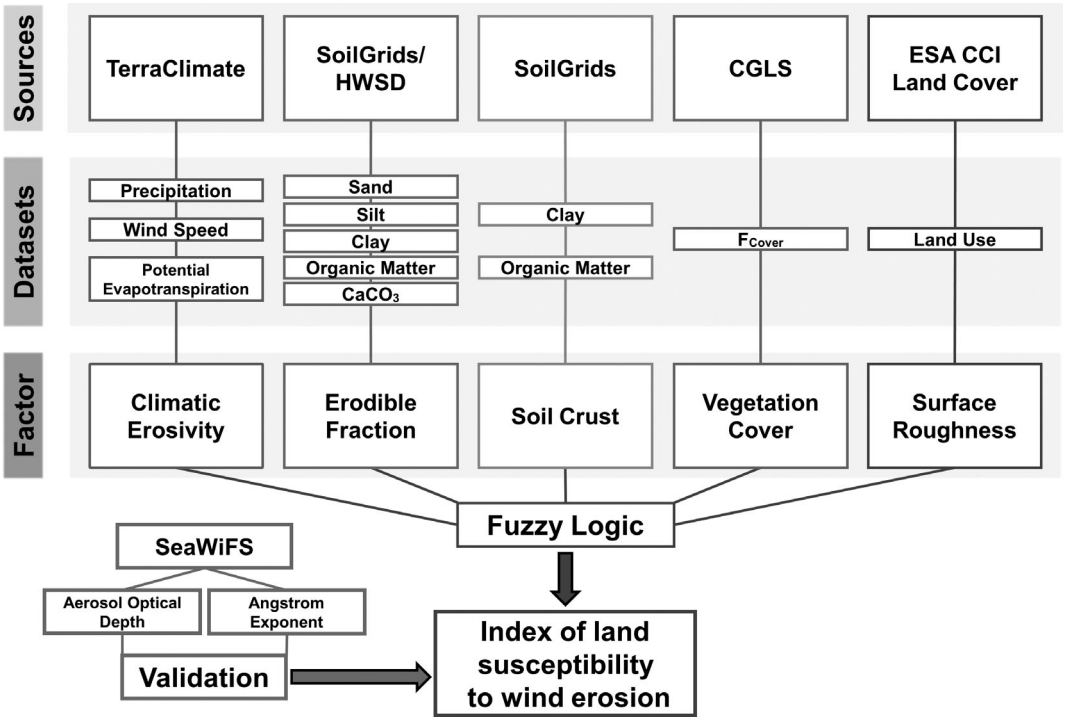

FIGURE 4 Workflow of methodological steps to calculate the index of land susceptibility to wind erosion and its validation process.

TABLE 1 Data sources with scale and time period.

Source	Dataset	Scale	Period/date
TerraClimate	Wind speed	4 × 4 km^2	Monthly mean for 2005–2019
	Precipitation		
	Potential evaporation (PET)		
ISRIC SoilGrids Database	Sand content	250 × 250 m^2	Latest release of 2020
	Silt content		
	Clay content		
	Organic matter content (OM)		
Harmonized World Soil Database (HWSD)	Calcium carbonate content	1 × 1 km^2	2012
Copernicus Global Land Service (CGLS)	Fraction of green vegetation	1 × 1 km^2	120-day value for 2005–2019
The European Space Agency (ESA)	Climate Change Initiative (CCI)	300 × 300 m^2	Annual for 2005–2019
	Land cover		
Sea-Viewing Wide Field-of-View Sensor (SeaWiFS)	Aerosol optical depth	0.5° × 0.5°	Daily values for 2005–2010
	Angstrom exponent		

with a 4 km resolution. TerraClimate uses an aided interpolation method, combining high-spatial resolution climatological normals from the WorldClim dataset (Fick & Hijmans, 2017) with other coarser datasets like the Climate Research Unit (Harris et al., 2014) and the Japanese 55-year reanalysis (Kobayashi et al., 2015). Technical details on the methodical background and the station-based ground truth validation are given in Abatzoglou et al. (2018).

2. Sand, silt, clay, and organic matter content are taken from the latest release from the ISRIC SoilGrids database. SoilGrids is a global, digital soil mapping system, producing a collection of soil property maps at 250 m resolution using global soil profile information and machine learning (de Sousa et al., 2020). Calcium carbonate content is derived from the Harmonized World Soil Database at 1 km resolution (FAO/IIASA/ISRIC/ISSCAS/JRC, 2012).
3. VC is derived from the fraction of green VC product from Copernicus Global Land Service for the period of 2005 to 2019. The 1 km grid-sized maps are generated from 10-day observations and made available as a mean 120-day value product.
4. The CCI Land Cover map was acquired from the European Space Agency. It is a high-resolution land cover map at 300 m grid size

based on Sentinel-2A observations as an annual product. The cloud-free reflectance composites were pre-processed with two classification algorithms: supervised Random Forest and unsupervised *Machine Learning*. Both approaches were then combined to generate the best outcome for a land cover class. For comparing wind erosion risk to the predominant land cover classification, relevant subdivision classes were combined into *shrubs cover*, *grassland*, *cropland*, *sparse vegetation*, and *bare areas* classes.

5. Daily aerosol optical depth (AOD) and angstrom exponent (AE) data are derived from SeaWiFS satellite SEASTAR with a resolution of 0.5° for the period of 2005–2010.

Every dataset was resampled to a 100 × 100 m^2 resolution in a UTM-based reference system, resulting in a pixel size of 1 ha. The ArcGIS resampling tool using the nearest neighbour method showed the best results. The downscaling was based on an upscaled grid of the land cover dataset used in the modeling process. The scale of 100 m, as a typical field unit, is suitable for comparison with other studies and thus meets the requirements for land use management.

3.3 | Climatic erosivity

The CE factor determines the average rate at which surface soil particles move relative to moisture content and average wind speed (Skidmore, 1986). We used a proposed model from Chepil et al. (1962) as a revised version by FAO (1979). It is best suited for arid regions, as the CE factor depends only on the wind speed when the rainfall amount approaches zero, while it is zero when the rainfall is equal to the potential evapotranspiration (Skidmore, 1986):

$$CE = 1/100 \sum_{i=1}^{i=12} u_i^3 \left(\frac{PET_i - P_i}{PET_i}\right) * d_i \quad (2)$$

Where: u_i is the average monthly wind speed (m s^{-1}) at 2 m height, PET_i is the monthly potential evapotranspiration (mm), P_i is the monthly precipitation (mm), and d_i represents the total number of days in month *i*.

3.4 | Wind-erodible fraction

The EF describes the susceptibility of a bare soil surface to wind-generated shear force due to its soil properties (Colazo & Buschiazzo, 2010). To determine the erodibility of soils, Chepil (1941) sieved samples into erodible and non-erodible fractions. Subsequent wind tunnel experiments showed that particles larger than 0.84 mm were stable under test conditions and considered non-erodible. The EF of soil is characterized by the portion of erodible aggregates of the top 25 mm of topsoil, with organic carbon and clay contents representing the main factors toward increasing aggregate stability by binding single particles (Fryrear, 1980; Skidmore & Layton, 1992). The calculation of the EF factor includes basic physical and chemical soil properties:

$$EF = \frac{29.09 + 0.31\,Sa + 0.17\,Si + 0.33\,\frac{Sa}{Cl} - 2.59\,OM - 0.95\,CaCO_3}{100} \quad (3)$$

Where: Sa is the sand content with a cutoff range from 5.5% to 93.6%, Si is the silt content with a cutoff range from 0.5% to 69.5%, Cl is the clay content with a cutoff range from 1.2% to 53%, OM is the organic matter content with a cutoff range from 0.18% to 4.79%, and $CaCO_3$ as the calcium carbonate content with an upper cutoff at 25.2% (Fryrear et al., 1994). The equation has not been verified for values outside of these ranges, thus the cutoffs were used if the datasets exceeded the validation limits (Fryrear et al., 1998).

3.5 | Soil crust

As most studies agree on the reductive effect of SCs on wind erosion (Belnap, 2003; Eldridge & Leys, 2003; Zhang et al., 2006), the SC factor is included in ILSWE, based on the regressed abrasion coefficient on clay and organic matter content (Fryrear et al., 1998):

$$SC = \frac{1}{1 + 0.0066\,(Cl)^2 + 0.021\,(OM)^2} \quad (4)$$

Where: Cl is the clay content with a cutoff range from 5% to 39.3% and OM is the organic matter content with a cutoff range from 0.32% to 4.74%. The limits of Equation (4) derive from wind tunnel tests on the resistance of soil aggregates and crusts to windblown sand (Hagen et al., 1992).

3.6 | Vegetation cover

The VC factor, as the ratio of vertically projected vegetation to the full extent of the area to be examined, can be expressed with the use of the fraction of VC (F_{Cover}), derived from the leaf area index and other canopy structural variables. Daily top of canopy reflectance is converted into estimates and in a second step filtered and smoothed by various inputs to distinguish between bare soil and the presence of vegetation (Verger et al., 2019).

3.7 | Surface roughness

Surface roughness refers to natural and man-made vertical irregularities of the earth's surface that decrease wind speed close to the ground in an inverse logarithmic relation (Sozzi et al., 1998). Therefore, SR elements affect near-surface aerodynamics and thus contribute to the reduction of aeolian transport. Since SR maps are not commonly available, it is possible to use land cover classes for an

estimation. We calculated the SR factor, by comparing annual 300 m gridded land cover maps with suggested roughness length values from Hansen (1993) (Table S11) and other sources (Floors et al., 2018; Markert et al., 2019).

3.8 | Validation by recognition of dust storms

Since long-term ground measurements of wind erosion data are not available, we used the SeaWiFS product's global daily AOD and AE to identify persistent dust sources derived from an estimate of the frequency of dust storms. After Ginoux et al. (2010), we calculated the estimation of dust storm frequency as the number of days with AOD > 0.25 and AE < 0.5. The annual mean frequency of dust storms was then ranked into five classes, similar to the wind erosion risk assessment map, by applying the Caspall-and-Jenks algorithm. An overlay analysis between the 15-year average wind erosion risk assessment and the 6-year mean annual frequency of dust storms, as a proxy for dust sources, was generated for an overall validation accuracy of our results.

4 | RESULTS

4.1 | Long-term wind erosion risk

Figure 5 summarizes the results of the period from 2005 to 2019 and shows the 15-year average of the wind erosion risk assessment. It has been derived with Equation (1) and subdivided into five classes. There is a clear west–east gradient, whose pattern correlates mainly with those of mean precipitation and wind speed. Around 91.7% of the area was classified with a very low to low susceptibility, while 5.7% show a medium risk and 2.5% a high to very high risk of wind erosion over that period. The areas most prone to wind erosion are located on the west coast of Namibia in the Namib Desert, with susceptible areas scattered around the western part of South Africa and Botswana, mainly the Kalahari basin. Impact factors, besides strong westerly winds, are sandy soils and sparse vegetation. The east of Southern Africa shows very low risk, largely due to high vegetation coverage by forests and permanent grass landscapes, as well as the presence of high precipitation throughout the year (Table S1).

As expected, elevated risk areas are only located in the desert and the Mediterranean shrubland biomes, in the case of the latter, caused by the high wind speeds near the coast. While there are areas in the savanna that are affected by wind erosion, the majority of its extent has a very low susceptibility and risk areas are situated around the border zones to more arid regions. The modelling results show no significant wind erosion risk in the montane grasslands and flooded grassland areas, with mangroves and lakes exclusively representing the low-risk classes, hence the latter was excluded from the supporting tables (Table S2).

In comparison with land cover classes, the modeling outcome displays that the 15-year mean annual wind erosion risk of cropland is very low to low. The reasoning is the long-term averaging time, which averages out times after harvest or fallow periods. Similarly, the shrubland and grassland classification display only a very low to low

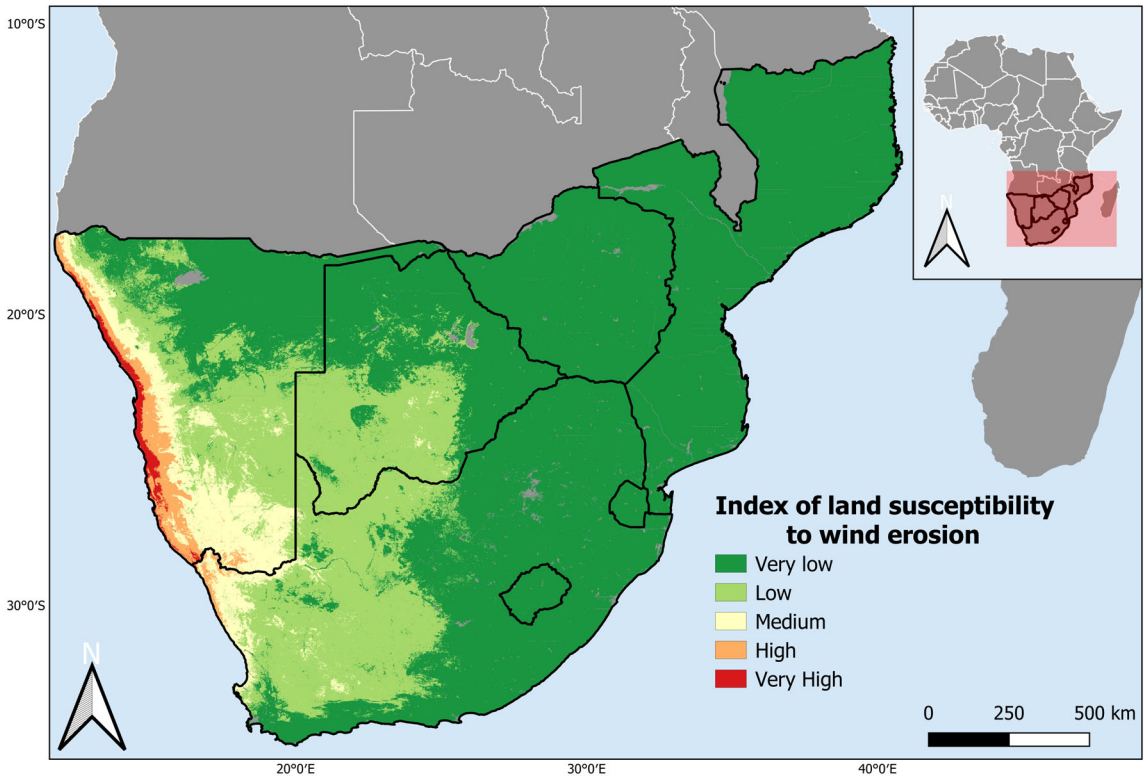

FIGURE 5 Susceptibility to wind erosion in Southern Africa as 15-year average. [Colour figure can be viewed at wileyonlinelibrary.com]

susceptibility to wind erosion, with grassland indicating a slightly elevated medium risk. On the other hand, the bare and sparse Vegetation classes represent around 95% (9.1 million ha) of the high to very high-risk areas, covering about 7.8% of the investigated region (Table S12). In context, only 0.3% of shrubland is affected by high susceptibility to wind erosion, representing an area of 0.4 million hectares (Table S6).

4.2 | Annual variability of the wind erosion risk

Figure 6 illustrates the annual variability of the wind erosion risk classes from 2005 to 2019. The results show a noticeable fluctuation between the classes with a slight upward trend of low to very high-risk areas, while the very low-class decrease cumulative to the other classes (Table S10). The annual average highlights 2007, 2013, 2015, and 2019, as years with an elevated wind erosion risk (Table S1, Figure S1).

The higher temporal resolution shows significantly more differentiation of the wind erosion risk depending on the biomes. While there is no significant deviation between the annual and 15-year mean for the forest, montane grassland classes, the savanna biome is subject to strong annual fluctuations. There is an area increase for the medium risk class up to 22 times in 2013 and 17 times in 2007, respectively. In addition, areas of increased risk become apparent in the exceptional years mentioned above. This trend solidifies when considering the flooded grassland and Mediterranean shrubland zones. Both ecoregions correlate in trends with the other classes, while the Mediterranean shrubland biome, situated on the southern coast of South Africa, depicts a major increase in wind erosion risk in 2017, compared to the 15-year average. As expected, the modeling results show a similar outcome across years for the desert zones compared to the 15-year mean, being the only class with a significant proportion in areas with a very high wind erosion susceptibility (Table S2).

When comparing the land cover classes with the annual wind erosion risk assessment, a trend emerges across all classes that highlight the climatically exceptional years 2007, 2011, 2013, 2015, 2019, and with restrictions, 2017. The cropland classification shows an increased medium risk in several years with a clear upward trend until 2017, whereby high and very high-risk areas are not deviating from the mean value, apart from 2017. The shrubland and grassland classifications show very little standard deviation of the low-risk categories from the 15-year mean, while the areas at considerable risk of wind erosion fluctuate strongly over the years. All annual modeled risk classes within the bare and sparse vegetation zones do not deviate significantly from the long-term mean (Table S6).

4.3 | Seasonal variability of the wind erosion risk

The inter-annual modeling of land susceptibility to wind erosion has been divided into three seasons, ranging from January to April (Sea1), May to August (Sea2), and September to December (Sea3), as the 120-day VC factor from CGLS does not allow a finer temporal resolution. There is a clear subdivision of the three time periods across years, with Sea1 having the lowest overall wind erosion risk, Sea2 having the highest proportion of medium to high-risk areas, and Sea3 being closest to the 15-year average in all area extent categories (Figure 7). Sea1 shows the greatest deviations in the very low and

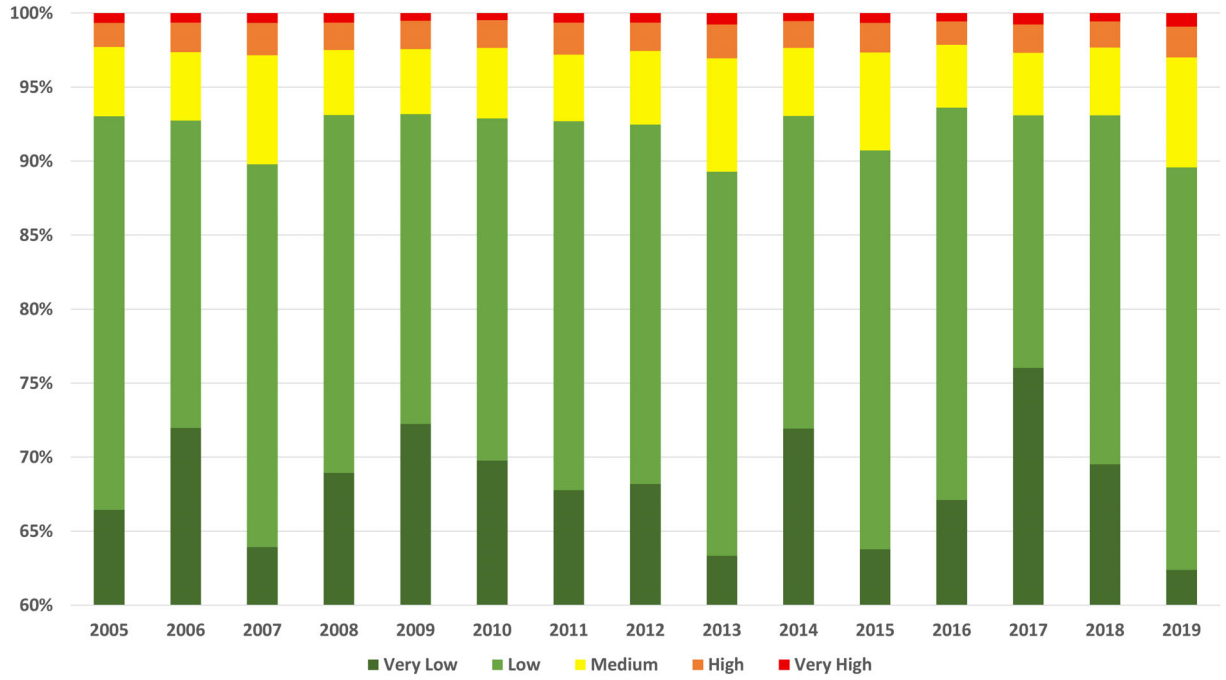

FIGURE 6 Annual variability of the wind erosion risk classified between 2005 and 2019. [Colour figure can be viewed at wileyonlinelibrary.com]

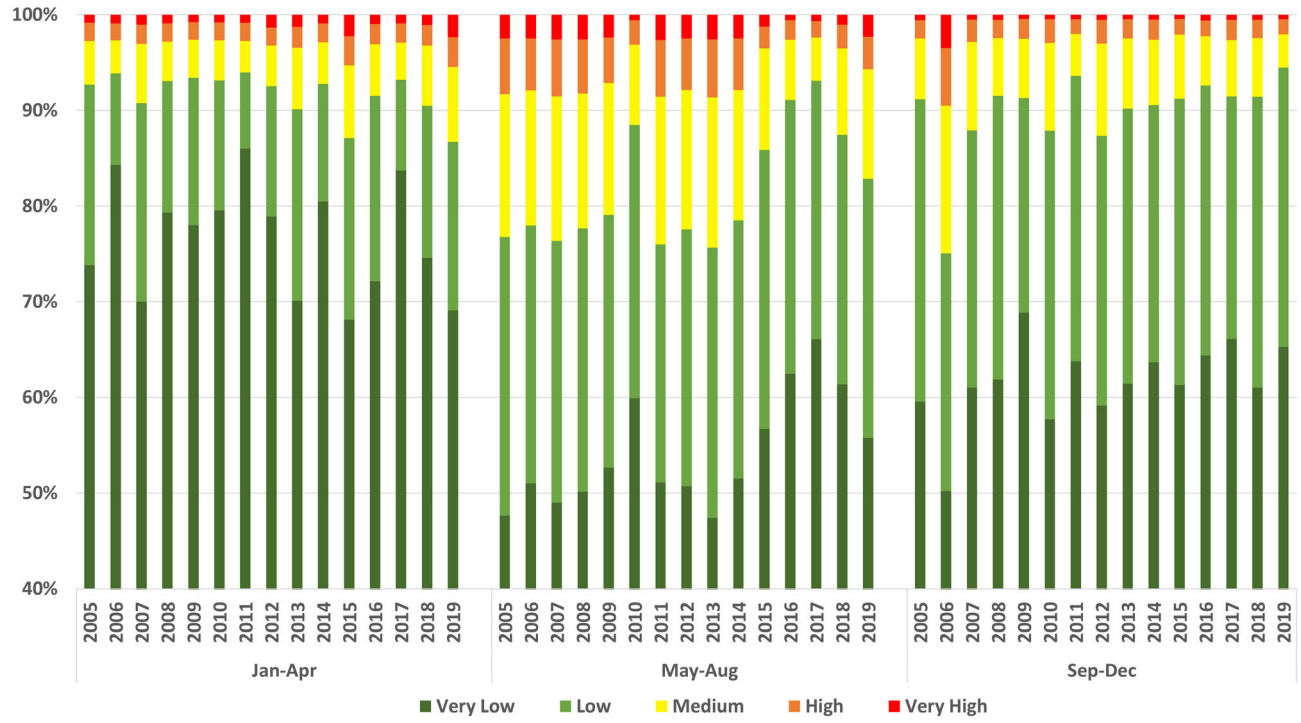

FIGURE 7 Seasonal variability of the wind erosion risk between 2005 and 2019 (Sea1: January–April; Sea2: May–August; and Sea3: September–December). [Colour figure can be viewed at wileyonlinelibrary.com]

medium classes over the years, with the years 2006, 2011, and 2017 standing out with the generally lowest risk of erosion within the 4-month periods. Overall, Sea2 has the highest wind erosion risk in the years up to the onset of a downward trend in 2015, with the 2013 season having the most extended share of risk areas. Sea3 is very consistent in the distribution of risk classes over the years, with 2007, 2010, and 2012 being noticeable outliers (Table S1). Although having the overall lowest proportions in high and very high-risk areas, the medium class takes up to 10% (40,000 km^2) of the total area, stretching far into the east of the Kalahari basin, Botswana (Figures S2–S4).

The breakdown of the results by biomes shows even more clearly the vulnerability of soils for wind erosion during the period from May to August. Both the flooded grassland and especially the savanna biome are subject to staggering increases of medium and elevated wind erosion risk in Sea2 compared to the annual means, with 2013 standing out. The results for the desert ecoregion illustrate a moderate to elevated susceptibility to wind erosion covering up to a maximum of 58% (779,311 km^2) of the biome extent, with the very low classification going as low as 5.7% (77,089 km^2) in 2013. It is worth noting that the risk areas account for 20.4% of the total study area during this specific time period. The forest and montane grassland biomes show no significant difference within the three seasons. Sea1 has the highest share of elevated risk areas for the Mediterranean shrubland region over the years. As it solely covers the southern tip of Africa, with the rainy season shifted toward the mid of the year, it results in Sea2 having the overall lowest susceptibility of soils to wind erosion and being very consistent in its results with no outlier years (Tables S3–S5).

Comparing the inter-annual modeling results with the distribution of the land cover classification it mainly highlights the most extensive regions, namely the shrubland and grassland classes. Both illustrate the highest proportion of medium to elevated land susceptibility to wind erosion from May to August, while fluctuating throughout the other two seasons. The bare and sparse vegetation classifications do not deviate significantly between the three seasons, while having the highest area percentage of medium to elevated risk within the classes. Since the vegetation in these land cover types changes only slightly over the course of the year, the temporal limitation of the data to a seasonal modelling approach has less influence on the result, when adding up the medium to a very high subdivision. Nearly all cropland areas have a very low or slight risk of wind erosion during all seasons, although there is an increase of medium risk during May to August pointing out the typical harvest period with a lower VC (Tables S7–S9).

5 | DISCUSSION

Our approach follows the validated model ILSWE that has been modified by Fenta et al. (2020) for application in East Africa, a region climatically similar to our study area. We adopted the validation methodology and compared the spatial and temporal derived wind erosion risk with the frequency of dust storms observed by satellites in that area. We got an overall accuracy of 65% for our study area (Table 2, Figure 8). The very low (80%) class has the highest validation accuracy, followed by the very high (40%) and low (38%) risk classification. Natural and anthropogenic fires occurred during the period of

TABLE 2 Error matrix: agreement of area in % between 15-year mean ILSWE and estimate for frequency of dust storms averaged between 2005 and 2010.

	Frequency of dust storms				
ILSWE	**Very low**	**Low**	**Medium**	**High**	**Very high**
Very low	53,8	11,7	1,4	0,2	0,0
Low	12,8	9,2	1,6	0,3	0,6
Medium	1,1	2,2	1,2	0,3	0,4
High	0,3	0,7	0,8	0,6	0,3
Very high	0,0	0,0	0,2	0,1	0,2
Overall accuracy	65%				

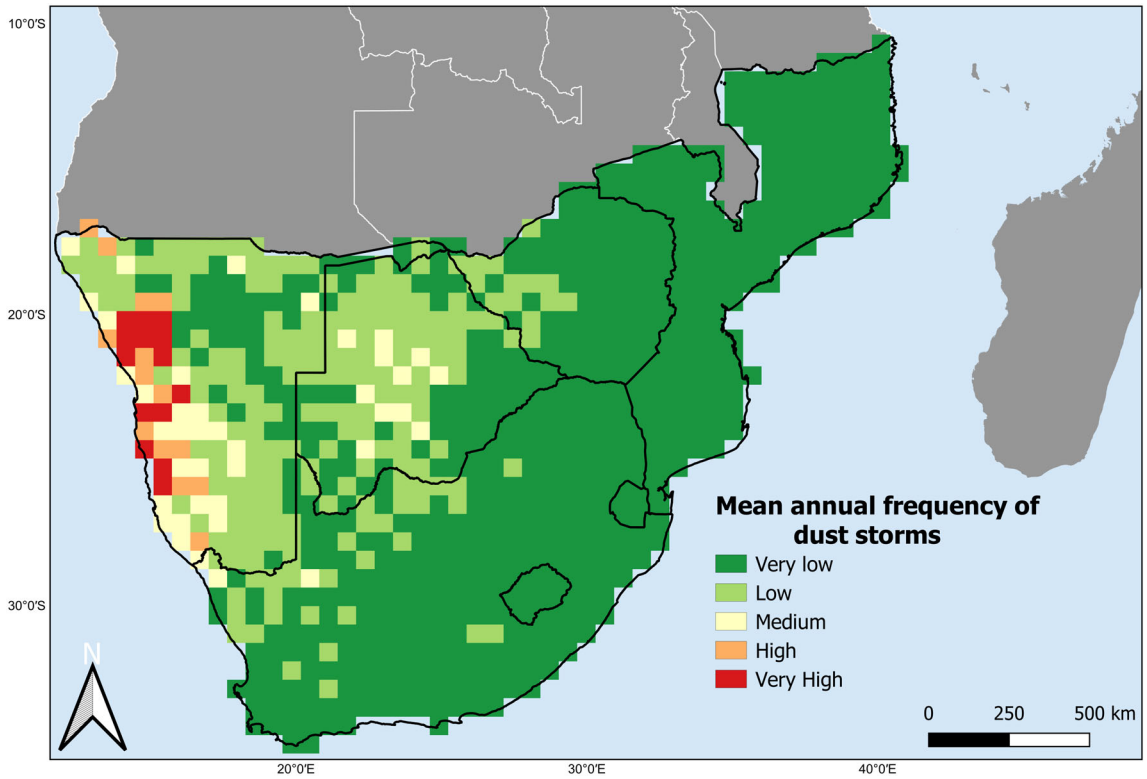

FIGURE 8 Estimate of mean annual frequency of dust storms derived from SeaWiFS daily data of aerosol optical depth (AOD) and angstrom exponent (AE) for the period between 2005 and 2010. [Colour figure can be viewed at wileyonlinelibrary.com]

the validation data and were falsely detected as dust sources (NASA, 2022). Corresponding time periods have been removed to prevent distortion of the spatial distribution of dust sources. As it was not possible to remove wildfire impact completely without affecting the actual classification of dust sources, the results can be considered satisfactory and are in line with other works (Fenta et al., 2016, 2020).

Zhao et al. (2021) investigated the impacts of climate change on wind erosion in Southern Africa by implementing the RWEQ to conduct an average wind erosion modulus for each year of the period 1991–2015, to perform a trend analysis. The fluctuation of the wind erosion dynamics from 2005 to 2015 are in good agreement with our annual modeled outcome. Our results in 2013 and 2015 show a similar expansion of risk areas compared to the extraordinary increase of 2007, which is not apparent in the same magnitude in the study of Zhao et al. (2021). Both model approaches use a similar methodology, but with different data sets. One reason for the deviations from 2010 onward could be the sharp drop in average wind speed that Zhao et al. (2021) determined over their investigation period, which is not in the order of magnitude of our TerraClimate product data series.

In recent years, several studies have been published on dust emissions and their sources in Southern Africa, with a specific focus on the Namib Desert (Dansie et al., 2017; Eckardt et al., 2020; Vickery et al., 2013; von Holdt et al., 2017). Accordingly, the main dust plume sources are situated in the Namib Desert and its coastal river catchments, the Kalahari pan belt, and the Botswana central pan. The spatial distribution of elevated risk areas of our results of the 15-year

mean wind erosion risk assessment are mainly distributed around the Namib Desert and its borders, while the inter-annual results indicate the Kalahari basin as a seasonal risk area.

In general, studies on wind erosion in Southern Africa are scarce. The increase of studies on erosion and dust generation in the region in recent years shows that the problem is being recognized and getting scientific attention. The processes of wind erosion vary considerably in their spatial and temporal distribution so large-scale studies can only give an approximate picture of the processes (Funk et al., 2004; Siegmund et al., 2018). While the spatial resolution can still be chosen relatively high even for larger areas in a GIS, the data availability sets limitations for the temporal resolution. Our wind erosion risk assessment follows an increasing temporal resolution of the period from 2005 to 2019, from the 15-year average to the annual and finally seasonal variability. The temporal variability is characterized by the dynamics of the climatic and vegetation factors. The graphical representations of said factors undermine the importance of vegetative ground cover to control wind erosion (Figures S5 and S9). While the influence of the climatic factor is mainly apparent on the southern coast, a region with less tropical influence and therefore characterized by greater climatic variance (Grieser et al., 2006), the patterns of wind erosion risk classes are directly dependent on the spatial distribution of the fractional vegetation index. These results are further reinforced if one considers the variability of the grassland and cropland classification, which in years with low vegetative cover led to a drastic increase in the medium and elevated risk classes. The grasslands cover most of the inland and are considered prone to irreversible degradation (Ravi et al., 2010). Southern African agricultural areas are susceptible to crop failures in climatically unfavourable years, such as maize cultivation, due to the dependency on monocultures and lack of crop diversification (FAO, 2021).

Our results for the seasonal wind erosion risk assessment are more differentiated than our annual outcomes (Table S1). The general trend shows a slight downward trend of medium to elevated risk classes, with Sea1 being more in line with the annual trend, Sea2 and with a lesser degree Sea3 representing the general trend, while having a larger extent of elevated risk classes respectively. The seasonal modeling outcome moderately represents the rainy, dry, and greening seasons, while the VC has a stronger influence on the results than the CE factor (Figures S6–S8 and S10–S12). Figure 9 shows the linear relationship of the CE factor toward the ILSWE results, while the VC factor has an overall higher impact with three distinct point clouds, representing the seasonal modeling outcome. Consequently, our results show that the period with the highest risk of wind erosion for agriculture is from January to August and the lowest protective effect of grassland is apparent from May to August. With rather low R^2 values for the annual and seasonal risk class trends, apart from the dry season between May and August, a future trend prediction on the wind erosion risk is associated with a high level of uncertainty (Table S10). A reason could be the variability and limitations of the fractional vegetation index. While climate data is readily available on a monthly basis, it is challenging to generate consistent, continuous vegetation data. In regions in and around the tropics clouding will produce noise and faulty surface reflectance (Hmimina et al., 2013). For our study region, the use of a 120-day composite vegetation index was necessary to provide at least one value per pixel, restricting the results to a seasonal index. Additionally, the fractional vegetation represents healthy leaf green, without fully considering the protective effect of dried and leafless vegetation (Chappell et al., 2018). This particularly affects the savanna landscapes with a natural dry cycle (Chidumayo, 2001). The SR factor ensures a certain consistency of the results, but overestimation of the wind erosion risk in dynamic drylands cannot be ruled out. In-depth trend analysis would require a more robust vegetation index as an input parameter, as well as dynamic estimates of SR, preferably with higher spatiotemporal resolution.

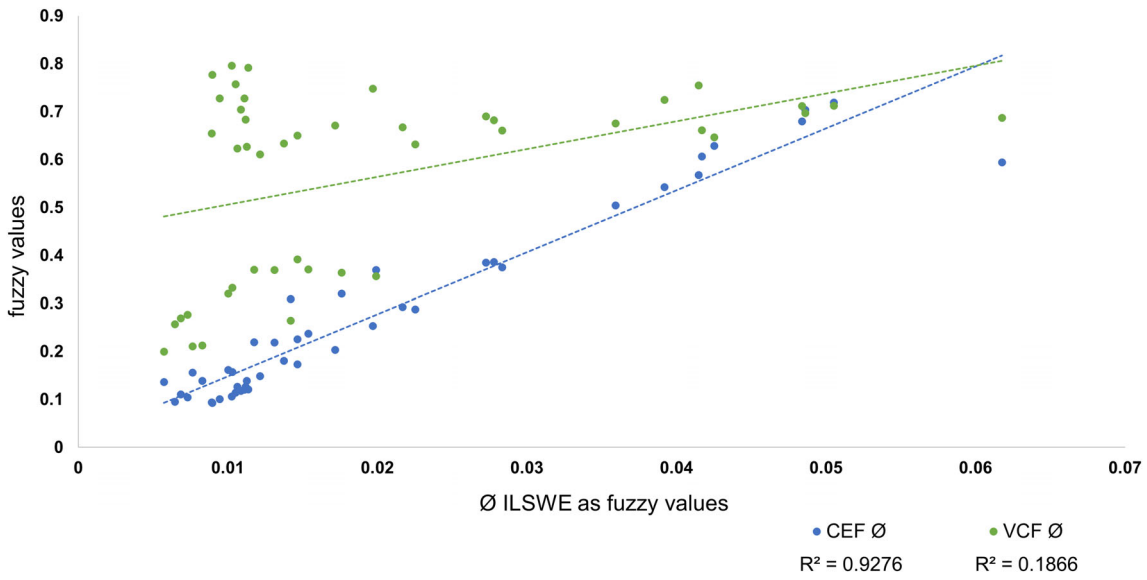

FIGURE 9 Comparison of the seasonal mean fuzzy values of ILSWE and the CEF and VCF. [Colour figure can be viewed at wileyonlinelibrary.com]

Past and recent studies show evidence, that droughts have become more intense and widespread in the region of Southern Africa (Fauchereau et al., 2003; Masih et al., 2014). Precipitation, or rather its absence, is the main driver of drought occurrence, however the inclusion of heat waves in drought projection is getting increasing attention, which will become more relevant in the context of climate change (Abiodun et al., 2012; Vicente-Serrano et al., 2011). Temperature is only indirectly represented in this study by potential evapotranspiration but has an impact on wind erosion too. Higher temperatures and low rainfall can result in limited vegetation growth, dry out soils and inhibit aggregation of particles, which increases the vulnerability of susceptible soils to wind erosion (Sharratt et al., 2013). There is evidence of a drastic increase in surface temperature on the African continent, on the order of twice the global temperature increase (Engelbrecht et al., 2015; Jones et al., 2012). Combined with an observed decrease in rainfall and a lengthening of the dry season since the late 60s, future drought scenarios anticipate significant pressures on the primarily rain-fed agricultural systems (Fauchereau et al., 2003; MacKellar et al., 2014; Niang et al., 2014). Our results show the highest share of medium and elevated risk classes in the years of 2007, 2013, 2015, and 2019, years when droughts and heatwaves afflicted large parts of Southern Africa (Nnopuechi, 2021). Apart from 2013, these were years with moderate to strong El Niño events, negatively affecting rainfall over the western part of Southern Africa and furthering high temperatures over long periods (Blamey et al., 2018; Pomposi et al., 2018). In 2017, the subdivided outcome for the Mediterranean shrubland zone shows the highest share of risk classes, the year with the most devastating drought in the last 100 years around the Cape of Africa (Pascale et al., 2020). Thegrasslands and cropland classification, being the most vulnerable to climatic influences, show the largest extent of medium to elevated risk areas in drought years (Table S6). These results are consistent with reported crop failures and the frequency of high fire danger days, resulting in bushfires in grasslands (Andela & van der Werf, 2014; Guimarães Nobre et al., 2019; Verschuur et al., 2021).

Given the overall trend of warming and decreasing average annual rainfall, wind erosion could become a more serious threat in the future. With limited resources and increasing population growth, pressures on agricultural systems may intensify, necessitating further conservation practices like the implementation of shelterbelts and agroforestry systems (Sheppard et al., 2020).

6 | CONCLUSIONS

The joint assessment of wind erosion for natural and anthropogenic-influenced areas makes it difficult to evaluate the effects on ecosystems. The very high risk in deserts associated with large amounts of erosion has to be evaluated differently than the often much lower dust emissions emitted from cropland, but leading to irreversible soil degradation. Agricultural areas are generally not threatened to a great degree in our results, but the extent of moderate and elevated wind erosion risk substantially rose in years of droughts. In addition, the temporal resolution of our modeling results is not sufficient to fully evaluate the wind erosion risk of highly dynamic agricultural systems and therefore demands further investigation. The dynamics of the annual and seasonal wind erosion risk were mainly influenced by the VC, with the CE factor having a regional impact. Under the consideration of a general warming trend, with a decrease in annual rainfall in the context of a changing climate, wind erosion could become a more problematic phenomenon in the future, demanding conservation policies for mitigation and adaptation. While our results identify hotspots of wind erosion, effective land management practices for controlling wind erosion are likely to vary locally and may include shelterbelts, revegetation, and similar sustainable measures to increase soil cover, biological diversity, and minimum soil disturbance. Field-based studies are therefore required for high-resolution mapping of target areas to develop individual adaptation strategies.

ACKNOWLEDGMENTS

This research was funded by the German Federal Ministry of Education and Research (BMBF), as part of the project "Agroforestry in Southern Africa – new pathways of innovative land use systems under a changing climate" (ASAP), grant number 01LL1803B. Open Access funding enabled and organized by Projekt DEAL.

CONFLICT OF INTEREST

The authors declare no conflicts of interest.

DATA AVAILABILITY STATEMENT

The data that support the findings of this study are openly available. The meteorological data is available at http://www.climatologylab.org/terraclimate (last access: 29 April 2021); the soil property data sets are available at https://www.isric.org (last access: 27 January 2021) and http://www.fao.org/soils-portal/data-hub/soil-maps-and-databases/harmonized-world-soil-database-v12 (last access: 14 December 2020); the fractional vegetation cover product is available at https://land.copernicus.eu/global/products/fcover (last access: 30 July 2021); the CCI Land Cover is available at https://www.esa-landcover-cci.org/ (last access: 04 September 2022); the unedited shapefile for the terrestrial ecoregions is available at: https://databasin.org (last access: 04 December 2020); and the daily aerosol optical depth and angstrom exponent data is available at: https://giovanni.gsfc.nasa.gov/giovanni/ (last access: 12 March 2022).

ORCID

Florian Kestel https://orcid.org/0000-0002-1464-5075

REFERENCES

Abatzoglou, J. T., Dobrowski, S. Z., Parks, S. A., & Hegewisch, K. C. (2018). TerraClimate, a high-resolution global dataset of monthly climate and climatic water balance from 1958–2015. *Scientific Data*, *5*, 12. https://doi.org/10.1038/sdata.2017.191

Abiodun, B. J., Adeyewa, Z. D., Oguntunde, P. G., Salami, A. T., & Ajayi, V. O. (2012). Modeling the impacts of reforestation on future climate in West Africa. *Theoretical and Applied Climatology*, *110*, 77–96. https://doi.org/10.1007/s00704-012-0614-1

Andela, N., & van der Werf, G. R. (2014). Recent trends in African fires driven by cropland expansion and El Niño to La Niña transition. *Nature Climate Change*, *4*, 791–795. https://doi.org/10.1038/nclimate2313

Belnap, J. (2003). Biological soil crusts and wind erosion. In J. Belnap & O. L. Lange (Eds.), *Biological soil crusts: Structure, function, and management*, *ecological studies* (pp. 339–347). Springer.

Blamey, R. C., Kolusu, S. R., Mahlalela, P., Todd, M. C., & Reason, C. J. C. (2018). The role of regional circulation features in regulating El Niño climate impacts over southern Africa: A comparison of the 2015/2016 drought with previous events. *International Journal of Climatology*, *38*, 4276–4295. https://doi.org/10.1002/joc.5668

Böhner, J., & Köthe, R. (2003). Soil regionalization and process modelling: Instruments for soil protection [Bodenregionalisierung und Prozessmodellierung: Instrumente für den Bodenschutz]. *Petermanns Geographische Mitteilungen*, *147*, 72–82. https://doi.org/10.1007/978-3-642-56475-8_25

Borrelli, P., Panagos, P., Ballabio, C., Lugato, E., Weynants, M., & Montanarella, L. (2016). Towards a pan-European assessment of land susceptibility to wind erosion. *Land Degradation & Development*, *27*, 1093–1105. https://doi.org/10.1002/ldr.2318

Burgess, N., World Wildlife Fund, W., D'Amico Hales, J., Underwood, E., Dinerstein, E., Olson, D., Itoua, I., Schipper, J., Ricketts, T., & Newman, K. (2004). *Terrestrial ecoregions of Africa and Madagascar: A conservation assessment*. Island Press.

Buschiazzo, D., & Zobeck, T. (2008). Validation of WEQ, RWEQ and WEPS wind erosion for different arable land management systems in the Argentinean pampas. *Earth Surface Processes and Landforms*, *33*, 1839–1850. https://doi.org/10.1002/esp.1738

Chappell, A., Baldock, J., & Sanderman, J. (2016). The global significance of omitting soil erosion from soil organic carbon cycling schemes. *Nature Climate Change*, *6*, 187–191. https://doi.org/10.1038/nclimate2829

Chappell, A., Webb, N. P., Guerschman, J. P., Thomas, D. T., Mata, G., Handcock, R. N., Leys, J. F., & Butler, H. J. (2018). Improving ground cover monitoring for wind erosion assessment using MODIS BRDF parameters, remote Sens. *Environment*, *204*, 756–768. https://doi.org/10.1016/j.rse.2017.09.026

Chepil, W. S. (1941). Relation of wind erosion to the dry aggregate structure of a soil. *Science in Agriculture*, *21*, 488–507. https://doi.org/10.4141/sa-1941-0029

Chepil, W. S., Siddoway, F. H., & Armbrust, D. V. (1962). Climatic factor for estimating wind erodibility of Fram fields. *Journal of Soil and Water Conservation*, *17*, 162–165.

Chidumayo, E. N. (2001). Climate and phenology of savanna vegetation in southern Africa. *Journal of Vegetation Science*, *12*(3), 347–354. https://doi.org/10.2307/3236848

Colazo, J. C., & Buschiazzo, D. E. (2010). Soil dry aggregate stability and wind erodible fraction in a semiarid environment of Argentina. *Geoderma*, *159*, 228–236. https://doi.org/10.1016/j.geoderma.2010.07.016

Dansie, A. P., Wiggs, G. F. S., Thomas, D. S. G., & Washington, R. (2017). Measurements of windblown dust characteristics and ocean fertilization potential: The ephemeral river valleys of Namibia. *Aeolian Research*, *29*, 30–41. https://doi.org/10.1016/j.aeolia.2017.08.002

de Sousa, L. M., Poggio, L., Batjes, N. H., Heuvelink, G. B. M., Kempen, B., Riberio, E., & Rossiter, D. (2020). SoilGrids 2.0: Producing quality-assessed soil information for the globe. *Soil Discussion*, *7*, 1–37. https://doi.org/10.5194/soil-2020-65

Department of Environmental Affairs. (2014). Long-term adaptation scenarios flagship research Programme (LTAS) for South Africa: Climate change adaptation: Perspectives for the southern African development community (SADC), Department of Environmental Affairs, Pretoria, South Africa.

D'Odorico, P., Bhattachan, A., Davis, K. F., Ravi, S., & Runyan, C. W. (2013). Global desertification: Drivers and feedbacks. *Advances in Water Resources*, *51*, 326–344. https://doi.org/10.1016/j.advwatres.2012.01.013

Eckardt, F. D., Bekiswa, S., Von Holdt, J. R., Jack, C., Kuhn, N. J., Mogane, F., Murray, J. E., Ndara, N., & Palmer, A. R. (2020). South Africa's agricultural dust sources and events from MSG SEVIRI. *Aeolian Research*, *47*, 12. https://doi.org/10.1016/j.aeolia.2020.100637

Eldridge, D. J., & Leys, J. F. (2003). Exploring some relationships between biological soil crusts, soil aggregation and wind erosion. *Journal of Arid Environments*, *53*, 457–466. https://doi.org/10.1006/jare.2002.1068

Engelbrecht, F., Adegoke, J., Bopape, M.-J., Naidoo, M., Garland, R., Thatcher, M., McGregor, J., Katzfey, J., Werner, M., Ichoku, C., & Gatebe, C. (2015). Projections of rapidly rising surface temperatures over Africa under low mitigation. *Environmental Research Letters*, *10*, 16. https://doi.org/10.1088/1748-9326/10/8/085004

FAO. (1979). A provisional methodology for soil degradation assessment Food and Agriculture Organization of the United Nations.

FAO. (2021). The impact of disasters and crises on agriculture and food security: 2021. FAO, Rome, Italy. https://doi.org/10.4060/cb3673en

FAO/IIASA/ISRIC/ISSCAS/JR. (2012). Harmonized World Soil Database (version 1.2). FAO, Rome, Italy and IIASA, Laxenburg, Austria. http://www.fao.org/3/aq361e/aq361e.pdf

Fauchereau, N., Trzaska, S., Rouault, M., & Richard, Y. (2003). Rainfall variability and changes in southern Africa during the 20th century in the global warming context. *Natural Hazards*, *29*, 139–154. https://doi.org/10.1023/A:1023630924100

Fenta, A. A., Tsunekawa, A., Haregeweyn, N., Poesen, J., Tsubo, M., Borrelli, P., Panagos, P., Vanmaercke, M., Broeckx, J., Yasuda, H., Kawai, T., & Kurosaki, Y. (2020). Land susceptibility to water and wind erosion risks in the East Africa region. *Science of the Total Environment*, *703*, 20. https://doi.org/10.1016/j.scitotenv.2019.135016

Fenta, A. A., Yasuda, H., Shimizu, K., Haregeweyn, N., & Negussie, A. (2016). Dynamics of soil erosion as influenced by watershed management practices: A case study of the Agula watershed in the semi-arid highlands of northern Ethiopia. *Environmental Management*, *58*, 889–905. https://doi.org/10.1007/s00267-016-0757-4

Fick, S. E., & Hijmans, R. J. (2017). WorldClim 2: New 1-km spatial resolution climate surfaces for global land areas. *International Journal of Climatology*, *37*, 4302–4315. https://doi.org/10.1002/joc.5086

Floors, R., Enevoldsen, P., Davis, N., Arnqvist, J., & Dellwick, E. (2018). From lidar scans to roughness maps for wind resource modelling in forested areas. *Wind Energy Science*, *3*, 353–370. https://doi.org/10.5194/wes-3-353-2018

Fryrear, D. W. (1980). *Tillage influences monthly wind erodibility of dryland sandy soils*. pp. 153–163. In Crop Production with Conservation in the 80s. Conference Proceedings, Chicago, IL. 1-2 Dec. American Society of Agricultural Engieneers, pp. 7–81.

Fryrear, D. W., Chen, W., & Lester, C. (2001). Revised wind erosion equation. *Annals of Arid Zone*, *40*, 265–279.

Fryrear, D. W., Krammes, C. A., Williamson, D. L., & Zobeck, T. M. (1994). Computing the wind erodible fraction of soils. *Journal of Soil and Water Conservation*, *49*, 183–188.

Fryrear, D. W., Saleh, A., Bilbro, J. D., Schromberg, H. M., Stout, J. E., & Zobeck, T. M. (1998). Revised wind erosion equation. USDA Technical Bulletins No 1.

Funk, R., & Reuter, H. I. (2006). Wind Erosion. In *Soil erosion in Europe* (pp. 563–582). John Wiley & Sons, Ltd.

Funk, R., Reuter, H. I., Hoffmann, C., Engel, W., & Öttl, D. (2008). Effect of moisture on fine dust emission from tillage operations on agricultural soils. *Earth Surface Processes and Landforms*, *33*, 1851–1863. https://doi.org/10.1002/esp.1737

Funk, R., Skidmore, E. L., & Hagen, L. J. (2004). Comparison of wind erosion measurements in Germany with simulated soil losses by WEPS. Environ. Model. Softw. *Modelling of Wind Erosion and Aeolian Processes*, *19*, 177–183. https://doi.org/10.1016/S1364-8152(03)00120-8

Ginoux, P., Garbuzov, D., & Hsu, N. C. (2010). Identification of anthropogenic and natural dust sources using moderate resolution imaging spectroradiometer (MODIS) deep blue level 2 data. *Journal of*

Geophysical Research – Atmospheres, *115*, 10. https://doi.org/10.1029/2009JD012398

Grieser, J., Gommes, R., & Bernardi, M. (2006). New LocClim - the local climate estimator of FAO. *Geophysical Research Abstracts*, *8*, 2.

Guimarães Nobre, G., Muis, S., Veldkamp, T. I. E., & Ward, P. J. (2019). Achieving the reduction of disaster risk by better predicting impacts of El Niño and La Niña. *Progress in Disaster Science*, *2*, 6. https://doi.org/10.1016/j.pdisas.2019.100022

Hagen, L. J., Skidmore, E. L., & Saleh, A. (1992). Wind erosion: Prediction of aggregate abrasion coefficients. *Transactions of ASAE*, *35*, 1847–1850. https://doi.org/10.13031/2013.28805

Hansen, F. (1993). Surface roughness lengths. ARL technical report US Army White Sands missile range. NM 88002-5501, pp. 51.

Harris, I., Jones, P. D., Osborn, T. J., & Lister, D. H. (2014). Updated high-resolution grids of monthly climatic observations – The CRU TS3.10 dataset. *International Journal of Climatology*, *34*, 623–642. https://doi.org/10.1002/joc.3711

Hijmans, R., Cameron, S., Parra, J., Jones, P., & Jarvis, A. (2005). Very high resolution interpolated climate surfaces of global land areas. *International Journal of Climatology*, *25*, 1965–1978. https://doi.org/10.1002/joc.1276

Hmimina, G., Dufrêne, E., Pontailler, J.-Y., Delpierre, N., Aubinet, M., Caquet, B., de Grandcourt, A., Burban, B., Flechard, C., Granier, A., Gross, P., Heinesch, B., Longdoz, B., Moureaux, C., Ourcival, J.-M., Rambal, S., Saint André, L., & Soudani, K. (2013). Evaluation of the potential of MODIS satellite data to predict vegetation phenology in different biomes: An investigation using ground-based NDVI measurements. *Remote Sensing of Environment*, *132*, 145–158. https://doi.org/10.1016/j.rse.2013.01.010

Huang, J., Yu, H., Guan, X., Wang, G., & Guo, R. (2016). Accelerated dryland expansion under climate change. *Nature Climate Change*, *6*, 166–171. https://doi.org/10.1038/nclimate2837

Huete, A., Didan, K., Miura, T., Rodriguez, E. P., Gao, X., & Ferreira, L. G. (2002). Overview of the radiometric and biophysical performance of the MODIS vegetation indices. *Remote Sensing of Environment*, *83*, 195–213. https://doi.org/10.1016/S0034-4257(02)00096-2

Jenks, G. F., & Caspall, F. C. (1971). Error on choroplethic maps: Definition, measurement, reduction. *Annals of the Association of American Geographers*, *61*, 217–244. https://doi.org/10.1111/j.1467-8306.1971.tb00779.x

Jones, P. D., Lister, D. H., Osborn, T. J., Harpham, C., Salmon, M., & Morice, C. P. (2012). Hemispheric and large-scale land-surface air temperature variations: An extensive revision and an update to 2010. *Journal of Geophysical Research-Atmospheres*, *117*, 29. https://doi.org/10.1029/2011JD017139

Kirui, O., & Mirzabaev, A. (2014). *Economics of land degradation in eastern Africa*. ZEF Working Paper Series, No. 128, University of Bonn, Center for Development Research (ZEF), Bonn. https://doi.org/10.13140/2.1.1442.2400

Klik, A. (2004). Wind erosion assessment in Austria using wind erosion equation and GIS. Proceddings OECD Expert Meet. Rome.

Kobayashi, S., Ota, Y., Harada, Y., Ebita, A., Moriya, M., Onoda, H., Onogi, K., Kamahori, H., Kobayashi, C., Endo, H., Miyaoka, K., & Takahashi, K. (2015). The JRA-55 reanalysis: General specifications and basic characteristics. *Journal of the Meteorological Society of Japan. Series II*, *93*, 5–48. https://doi.org/10.2151/jmsj.2015-001

Kotze, I., & Rose, M. (2015). Farming facts and futures: Reconnecting South Africa's food systems to its ecosystems. WWF-SA. http://awsassets.wwf.org.za/downloads/wwf006_ffl_report_low_res.pdf

Le Roux, J., Morgenthal, T., Malherbe, J., Pretorius, D., & Sumner, P. (2008). Water erosion prediction at a national scale for South Africa. *Water SA*, *34*, 305–314. https://doi.org/10.4314/wsa.v34i3.180623

Le Roux, J., Newby, T., & Sumner, P. (2007). Monitoring soil erosion in South Africa at a regional scale: Review and recommendations. *South African Journal of Science*, *103*, 329–335. http://hdl.handle.net/2263/5782

MacKellar, N., New, M., & Jack, C. (2014). Observed and modelled trends in rainfall and temperature for South Africa: 1960-2010. *South African Journal of Science*, *110*, 1–13. https://doi.org/10.1590/sajs.2014/20130353

Markert, A., Griffin, R., Knupp, K., Molthan, A., & Coleman, T. (2019). A spatial pattern analysis of land surface roughness heterogeneity and its relationship to the initiation of weak tornadoes. *Earth Interactions*, *23*, 1–28. https://doi.org/10.1175/EI-D-18-0010.1

Masih, I., Maskey, S., Mussá, F. E. F., & Trambauer, P. (2014). A review of droughts on the African continent: A geospatial and long-term perspective. *Hydrology and Earth System Sciences*, *18*, 3635–3649. https://doi.org/10.5194/hess-18-3635-2014

McBratney, A. B., & Odeh, I. O. A. (1997). Application of fuzzy sets in soil science: Fuzzy logic, fuzzy measurements and fuzzy decisions. *Geoderma*, *77*, 85–113. https://doi.org/10.1016/S0016-7061(97)00017-7

Montanarella, L., Pennock, D. J., McKenzie, N., Badraoui, M., Chude, V., Baptista, I., Mamo, T., Yemefack, M., Singh Aulakh, M., Yagi, K., Young Hong, S., Vijarnsorn, P., Zhang, G.-L., Arrouays, D., Black, H., Krasilnikov, P., Sobocká, J., Alegre, J., Henriquez, C. R., … Vargas, R. (2016). World's soils are under threat. *The Soil*, *2*, 79–82. https://doi.org/10.5194/soil-2-79-2016

Montgomery, D. R. (2007). Soil erosion and agricultural sustainability. *Proceedings of the National Academy of Sciences*, *104*, 13268–13272. https://doi.org/10.1073/pnas.0611508104

Munson, S., Belnap, J., & Okin, G. (2011). Responses of wind erosion to climate-induced vegetation changes on the Colorado Plateau. *Proceedings of the National Academy of Sciences of the United States of America*, *108*, 3854–3859. https://doi.org/10.1073/pnas.1014947108

NASA. (2022). FIRE & Aerosol optical depth. https://earthobservatory.nasa.gov/global-maps/MOD14A1_M_FIRE/MODAL2_M_AER_OD

Nerger, R., Funk, R., Cordsen, E., & Fohrer, N. (2017). Application of a modeling approach to designate soil and soil organic carbon loss to wind erosion on long-term monitoring sites (BDF) in northern Germany. *Aeolian Research*, *25*, 135–147. https://doi.org/10.1016/j.aeolia.2017.03.006

New, M., Hewitson, B., Stephenson, D., Tsiga, A., Kruger, A., Manhique, A., Gomez, B., Coelho, S., Masisi, D., Kululanga, E., Mbambalala, E., Adesina, F., Saleh, H., Kanyanga, J. K., Adosi, J., Bulane, L., Fortunata, L., Mdoka, M., & Lajoie, R. (2006). Evidence of trends in daily climate extremes over southern and West Africa. *Journal of Geophysical Research*, *111*, 11. https://doi.org/10.1029/2005JD006289

Niang, I., Ruppel, O. C., Abdrabo, M. A., Essel, A., Lennard, C., Padgham, J., & Urquhart, P. (2014). Africa. In *Climate change 2014: Impacts, adaptation, and vulnerability. Part B: Regional aspects. Contribution of working group II to the fifth assessment report of the Intergovernmental Panel on Climate Change*. Cambridge University Press.

Nnopuechi, J. (2021). The history of recent droughts in Africa (1980-2020) consequences, responses and lessons learned. Research Report, University of Gothenburg. https://secaangola.hypotheses.org/files/2021/02/Jennifer-Nnopuechi-2021-History-of-Recent-Droughts-in-Africa-1980-2020-REPORT.pdf

Obalum, S., Buri, M., Nwite, J., Hermansah, H., Watanabe, Y., Igwe, C., & Wakatsuki, T. (2012). Soil degradation-induced decline in productivity of sub-Saharan African soils: The prospects of looking downwards the lowlands with the Sawah Ecotechnology. *Applied and Environmental Soil Science*, *2012*, 1–10. https://doi.org/10.1155/2012/673926

Olson, D. M., Dinerstein, E., Wikramanayake, E. D., Burgess, N. D., Powell, G. V. N., Underwood, E. C., D'Amico, J. A., Strand, H. E., Morrison, J. C., Loucks, C. J., Allnutt, T. F., Lamoreux, J. F., Ricketts, T. H., Itoua, I., Wettengel, W. W., Kura, Y., Hedao, P., & Kassem, K. (2001). Terrestrial ecoregions of the world: A new map of

life on Earth. *Bioscience*, *51*, 933–938. https://doi.org/10.1641/00063568(2001)051[0933:TEOTWA]2.0.CO;2

Osborn, T. J., & Jones, P. D. (2014). The CRUTEM4 land-surface air temperature data set: Construction, previous versions and dissemination via Google earth. *Earth System Science Data*, *6*, 61–68. https://doi.org/10.5194/essd-6-61-2014

Pascale, S., Kapnick, S. B., Delworth, T. L., & Cooke, W. F. (2020). Increasing risk of another Cape Town "day zero" drought in the 21st century. *Proceedings of the National Academy of Sciences*, *117*, 29495–29503. https://doi.org/10.1073/pnas.2009144117

Philippon, N., Rouault, M., Richard, Y., & Favre, A. (2012). The influence of ENSO on South Africa winter rainfall. *International Journal of Climatology*, *32*, 2333–2347. https://doi.org/10.1002/joc.3403

Pomposi, C., Funk, C., Shukla, S., Harrison, L., & Magadzire, T. (2018). Distinguishing southern Africa precipitation response by strength of El Niño events and implications for decision-making. *Environmental Research Letters*, *13*, 12. https://doi.org/10.1088/1748-9326/aacc4c

Ravi, S., Breshears, D. D., Huxman, T. E., & D'Odorico, P. (2010). Land degradation in drylands: Interactions among hydrologic–aeolian erosion and vegetation dynamics. *Geomorphology*, *Geomorphology and Vegetation: Interactions*, *Dependencies*, *and Feedback Loops*, *116*, 236–245. https://doi.org/10.1016/j.geomorph.2009.11.023

Ravi, S., D'Odorico, P., Breshears, D., Field, J., Goudie, A., Huxman, T., Li, L., Okin, G., Swap, R., Thomas, A., Van Pelt, R., Whicker, J., & Zobeck, T. M. (2011). Aeolian process and the biosphere. *Reviews of Geophysics*, *49*, 1–45. https://doi.org/10.1029/2010RG000328

Rienecker, M. M., Suarez, M. J., Gelaro, R., Todling, R., Bacmeister, J., Liu, E., Bosilovich, M. G., Schubert, S. D., Takacs, L., Kim, G.-K., Bloom, S., Chen, J., Collins, D., Conaty, A., da Silva, A., Gu, W., Joiner, J., Koster, R. D., Lucchesi, R., … Woollen, J. (2011). MERRA: NASA's modern-era retrospective analysis for research and applications. *Journal of Climate*, *24*, 3624–3648. https://doi.org/10.1175/JCLI-D-11-00015.1

Shao, Y. (2008). *Physics and modelling of wind erosion*, 2. Rev. & Exp. ed, Atmospheric and oceanographic sciences library. Springer.

Shao, Y., Wyrwoll, K.-H., Chappell, A., Huang, J., Lin, Z., McTainsh, G. H., Mikami, M., Tanaka, T. Y., Wang, X., & Yoon, S. (2011). Dust cycle: An emerging core theme in earth system science. *Aeolian Research*, *2*, 181–204. https://doi.org/10.1016/j.aeolia.2011.02.001

Sharratt, B. S., Vaddella, V. K., & Feng, G. (2013). Threshold friction velocity influenced by wetness of soils within the Columbia Plateau. *Aeolian Research*, *9*, 175–182. https://doi.org/10.1016/j.aeolia.2013.01.002

Sheppard, J. P., Bohn Reckziegel, R., Borrass, L., Chirwa, P. W., Cuaranhua, C. J., Hassler, S. K., Hoffmeister, S., Kestel, F., Maier, R., Mälicke, M., Morhart, C., Ndlovu, N. P., Veste, M., Funk, R., Lang, F., Seifert, T., du Toit, B., & Kahle, H.-P. (2020). Agroforestry: An appropriate and sustainable response to a changing climate in southern Africa? *Sustainability*, *12*, 31. https://doi.org/10.3390/su12176796

Siegmund, N., Funk, R., Koszinsky, S., Buschiazzo, D. E., & Sommer, M. (2018). Effects of low-scale landscape structures on aeolian transport processes on arable land. *Aeolian Research*, *32*, 181–191. https://doi.org/10.1016/j.aeolia.2018.03.003

Skidmore, E. L. (1986). Wind erosion climatic erosivity. *Climatic Change*, *9*, 195–208. https://doi.org/10.1007/BF00140536

Skidmore, E. L., & Layton, J. B. (1992). Dry-soil aggregate stability as influenced by selected soil properties. *Soil Science Society of America Journal*, *56*, 557–561. https://doi.org/10.2136/sssaj1992.03615995005600020034x

Sozzi, R., Favaron, M., & Georgiadis, T. (1998). Method for estimation of surface roughness and similarity function of wind speed vertical profile. *Journal of Applied Meteorology*, *37*, 461–469. https://doi.org/10.1175/1520-0450(1998)037<0461:MFEOSR>2.0.CO;2

Sterk, G., Herrmann, L., & Bationo, A. (1996). Wind-blown nutrient transport and soil productivity changes in Southwest Niger. *Land Degradation & Development*, *7*, 325–335. https://doi.org/10.1002/(SICI)1099-145X(199612)7:4<325::AID-LDR237>3.0.CO;2-Q

Tatarko, J., Sporcic, M. A., & Skidmore, E. L. (2013). A history of wind erosion prediction models in the United States Department of Agriculture prior to the wind erosion prediction system. *Aeolian Research*, *10*, 3–8. https://doi.org/10.1016/j.aeolia.2012.08.004

Tsoar, H. (1994). Bagnold, R.A. 1941: The physics of blown sand and desert dunes. *Progress in Physical Geography-Earth and Environment*, *18*, 91–96. https://doi.org/10.1177/030913339401800105

UNEP. (2015). The economics of land degradation in Africa: Benefits of action outweigh the costs. UNEP. www.eld-initiative.org

USDA. (2002). National agronomy manual. https://www.nrcs.usda.gov/Internet/FSE_DOCUMENTS/stelprdb1043208.pdf

Verger, A., Baret, F., & Weiss, M. (2019). COPERNICUS global land operations "vegetation and energy." I1.41. https://land.copernicus.eu/global/sites/cgls.vito.be/files/products/CGLOPS1_ATBD_FCOVER1km-V2_I1.41.pdf

Verschuur, J., Li, S., Wolski, P., & Otto, F. E. L. (2021). Climate change as a driver of food insecurity in the 2007 Lesotho-South Africa drought. *Scientific Reports*, *11*, 3852. https://doi.org/10.1038/s41598-021-83375-x

Vicente-Serrano, S. M., López-Moreno, J. I., Drumond, A., Gimeno, L., Nieto, R., Morán-Tejeda, E., Lorenzo-Lacruz, J., Beguería, S., & Zabalza, J. (2011). Effects of warming processes on droughts and water resources in the NW Iberian -peninsula (1930–2006). *Climate Research*, *48*, 203–212. https://doi.org/10.3354/cr01002

Vickery, K. J., Eckardt, F. D., & Bryant, R. G. (2013). A sub-basin scale dust plume source frequency inventory for southern Africa, 2005–2008. *Geophysical Research Letters*, *40*, 5274–5279. https://doi.org/10.1002/grl.50968

von Holdt, J. R., Eckardt, F. D., & Wiggs, G. F. S. (2017). Landsat identifies aeolian dust emission dynamics at the landform scale. *Remote Sensing of Environment*, *198*, 229–243. https://doi.org/10.1016/j.rse.2017.06.010

Webb, N. P., Edwards, B. L., & Pierre, C. (2020). Wind erosion in anthropogenic environments. In *Reference module in earth systems and environmental sciences*. Elsevier.

Weinzierl, T., Wehberg, J., Böhner, J., & Conrad, O. (2016). Spatial assessment of land degradation risk for the Okavango River catchment, Southern Africa. *Land Degradation & Development*, *27*, 281–294. https://doi.org/10.1002/ldr.2426

Wever, N. (2012). Quantifying trends in surface roughness and the effect on surface wind speed observations. *Journal of Geophysical Research-Atmospheres*, *117*, 14. https://doi.org/10.1029/2011JD017118

Wiesmeier, M., Steffens, M., Mueller, C. W., Kölbl, A., Reszkowska, A., Peth, S., Horn, R., & Kögel-Knabner, I. (2012). Aggregate stability and physical protection of soil organic carbon in semi-arid steppe soils. *European Journal of Soil Science*, *63*, 22–31. https://doi.org/10.1111/j.1365-2389.2011.01418.x

Wiggs, G., & Holmes, P. (2011). Dynamic controls on wind erosion and dust generation on west-Central Free State agricultural land, Southern Africa. *Earth Surface Processes and Landforms*, *36*, 827–838. https://doi.org/10.1002/esp.2110

Woodruff, N. P., & Siddoway, F. H. (1965). A wind erosion equation. *Soil Science Society of America Journal*, *29*, 602–608. https://doi.org/10.2136/sssaj1965.03615995002900050035x

Yan, H., Wang, S., Wang, C., Zhang, G., & Patel, N. (2005). Losses of soil organic carbon under wind erosion in China. *Global Change Biology*, *11*, 828–840. https://doi.org/10.1111/j.1365-2486.2005.00950.x

Zabel, F., Putzenlechner, B., & Mauser, W. (2014). Global agricultural land resources – A high resolution suitability evaluation and its perspectives until 2100 under climate change conditions. *PLoS One*, *9*, 12. https://doi.org/10.1371/journal.pone.0107522

Zadeh, L. A. (1965). Fuzzy sets. *Information and Control*, *8*, 338–353. https://doi.org/10.1016/S0019-9958(65)90241-X

Zhang, Y. M., Wang, H. L., Wang, X. Q., Yang, W. K., & Zhang, D. Y. (2006). The microstructure of microbiotic crust and its influence on wind erosion for a sandy soil surface in the Gurbantunggut Desert of northwestern China. *Geoderma*, *132*, 441–449. https://doi.org/10.1016/j.geoderma.2005.06.008

Zhao, C., Zhang, H., Wang, M., Jiang, H., Peng, J., & Wang, Y. (2021). Impacts of climate change on wind erosion in southern Africa between 1991 and 2015. *Land Degradation & Development*, *32*, 2169–2182. https://doi.org/10.1002/ldr.3895

Zheng, X. (2009). *Mechanics of wind-blown sand movements, environmental science*. Springer-Verlag. https://doi.org/10.1007/978-3-540-88254-1

SUPPORTING INFORMATION

Additional supporting information can be found online in the Supporting Information section at the end of this article.

How to cite this article: Kestel, F., Wulf, M., & Funk, R. (2023). Spatiotemporal variability of the potential wind erosion risk in Southern Africa between 2005 and 2019. *Land Degradation & Development*, *34*(10), 2945–2960. https://doi.org/10.1002/ldr.4659